

## Model Projections of an Imminent Transition to a More Arid Climate in Southwestern North America

Richard Seager,<sup>1</sup> Mingfang Ting,<sup>1</sup> Isaac Held,<sup>2,3</sup> Yochanan Kushnir,<sup>1</sup> Jian Lu,<sup>4</sup> Gabriel Vecchi,<sup>2</sup> Huei-Ping Huang,<sup>1</sup> Nili Harnik,<sup>5</sup> Ants Leetmaa,<sup>2</sup> Ngar-Cheung Lau,<sup>2,3</sup> Cuihua Li,<sup>1</sup> Jennifer Velez,<sup>1</sup> Naomi Naik<sup>1</sup>

<sup>1</sup>Lamont Doherty Earth Observatory of Columbia University, Palisades, NY, USA. <sup>2</sup>NOAA Geophysical Fluid Dynamics Laboratory, Princeton, NJ, USA. <sup>3</sup>Program in Atmospheric and Oceanic Sciences, Department of Geosciences, Princeton University, Princeton, NJ, USA. <sup>4</sup>National Center for Atmospheric Research, Boulder, CO, USA. <sup>5</sup>Tel Aviv University, Tel Aviv, Israel.

**How anthropogenic climate change will impact hydroclimate in the arid regions of Southwestern North America has implications for the allocation of water resources and the course of regional development. Here we show that there is a broad consensus amongst climate models that this region will dry significantly in the 21st century and that the transition to a more arid climate should already be underway. If these models are correct, the levels of aridity of the recent multiyear drought, or the Dust Bowl and 1950s droughts, will, within the coming years to decades, become the new climatology of the American Southwest.**

The Third Assessment Report of the Intergovernmental Panel on Climate Change (IPCC) reported that the average of all the participating models showed a general decrease in rainfall in the subtropics during the 21st century although there was also considerable disagreement amongst the models (1). Subtropical drying accompanying rising CO<sub>2</sub> is also found in the models participating in the second Coupled Model Intercomparison Project (2). Here we examine future subtropical drying by analyzing the time history of precipitation in 19 climate models participating in the Fourth Assessment Report (AR4) of the IPCC (3). The future climate projections followed the A1B emissions scenario (4) in which CO<sub>2</sub> emissions increase until about 2050 and decrease modestly thereafter leading to a CO<sub>2</sub> concentration of 720 ppm in 2100. We also analyzed the simulations by these models of the 1860–2000 period in which the models were forced by the known history of trace gases and, with some variation amongst the models, estimated changes of solar irradiance, volcanic and anthropogenic aerosols and land use. These simulations provide initial conditions for the 21st century climate projections. For each model, climatologies were computed over the 1950–2000 period by averaging over all the simulations available for each model. All climate changes shown are departures from this climatology.

We define an area (shown as a box on Fig. 4) called 'The Southwest' including all land between 125°W and 95°W and 25°N and 40°N that incorporates the southwestern United

States and parts of northern Mexico. Fig. 1 shows the modeled history and future of the annual mean precipitation minus evaporation ( $P-E$ ) averaged over this region for the period common to all the models, 1900–2098. The median, 25th and 75th percentiles of the model  $P-E$  distribution and the median of  $P$  and  $E$  are shown. For cases in which there were multiple simulations with a single model these were averaged together before computing the distribution.  $P-E$  equals the moisture convergence by the atmospheric flow and, over land, the amount of water that goes into runoff.

In the multi-model ensemble mean there is a transition to a sustained drier climate that begins in the late 20th and early 21st centuries. In the ensemble mean both  $P$  and  $E$  decrease but the former by a larger amount.  $P-E$  primarily reduces in winter when  $P$  reduces and  $E$  is unchanged or modestly increased while in summer both  $P$  and  $E$  decrease (not shown). The annual mean reduction in  $P$  for this region, calculated from rain gauge data within the Global Historical Climatology Network, was 0.09 mm/day between 1932 and 1939 (the Dust Bowl drought) and 0.13 mm/day between 1948 and 1957 (the 1950s Southwest drought). The ensemble median reduction in  $P$  that drives the reduction in  $P-E$  reaches 0.1 mm/day in mid-century and one quarter of the models reach this in the early part of the current century.

Figure 2 shows for the 19 models the annual mean  $P-E$  difference between 20 year periods in the 21st century and the model's 1950–2000 climatology. Almost all models have a drying trend in the American Southwest and consistently so throughout the century. Only one of the 19 models has a trend to a wetter climate. Of the total of 49 individual projections conducted with the 19 models, even as early as the 2021 to 2040 period, only 3 show a shift to a wetter climate. Examples of modeled history and future precipitation for single simulations of four individual models are shown in Fig. 3 and provide an idea of potential trajectories towards the more arid climate.

Figure 4 shows (contours, all panels) a map of the change in  $P-E$  for the decades between 2021 and 2040 minus the

1950–2000 period for one of the IPCC models: the Geophysical Fluid Dynamics Laboratory climate model CM2.1 (5). In general, large regions of the relatively dry subtropics dry further while wetter higher latitude regions become wetter still. In addition to the American Southwest, the Southern Europe-Mediterranean-Middle East region also experiences a severe drying. This pattern of subtropical drying and moistening at higher latitudes is a robust feature of current projections with different models of future climate (6).

The change ( $\delta$ ) in  $P-E$  (in m/s) is balanced by a change in atmospheric moisture convergence, viz.:

$$\rho_w g \delta(P-E) = -\delta \left( \int_0^{p_s} \nabla \cdot (\overline{uq}) dp + \int_0^{p_s} \nabla \cdot (\overline{u'q'}) dp \right) \quad (1)$$

Overbars indicate monthly means and primes departures from the monthly mean,  $\rho_w$  is the density of water. The change in moisture convergence can be divided into contributions from the 'mean flow' and from 'eddies'. In the former the atmospheric flow ( $\overline{u}$ ) and the moisture ( $\overline{q}$ ) are averaged over a month before computing the moisture transport, while the latter is primarily associated with the highly variable wind ( $u'$ ) and moisture ( $q'$ ) fields within storm systems. The moisture convergence is integrated over pressure ( $p$ ) from the top of the atmosphere ( $p = 0$ ) to the surface ( $p_s$ ). The mean wind and humidity fields in Eq. 1 can be taken to be their climatological fields. (The rectification of interannual variability in the monthly mean flow and moisture fields is found to be negligible.) Changes in the mean flow contribution can, in turn, be approximated by one part associated with the 1950–2000 climatological circulation ( $\overline{u^P}$ ) operating on the increase in climatological atmospheric humidity ( $\delta \overline{q}$ , a consequence of atmospheric warming) and another part due to the change in circulation climatology ( $\delta \overline{u}$ ) operating on the 1950–2000 atmospheric humidity climatology ( $\overline{q^P}$ ). The nonlinear term involving changes in both the mean flow and moisture field is found to be relatively small (not shown). Hence Eq. 1 can be approximated by:

$$\rho_w g \delta(P-E) \sim -\int_0^{p_s} \nabla \cdot (\overline{q^P} \delta \overline{u} + \overline{u^P} \delta \overline{q}) dp - \delta \int_0^{p_s} \nabla \cdot (\overline{u'q'}) dp \quad (2)$$

We therefore think in terms of a three-fold decomposition of  $P-E$ , as displayed in Fig. 4 (colors) for the GFDL CM2.1 model: a contribution from the change in mean circulation, a contribution from the change in mean humidity, and a contribution from eddies.

The mean flow convergence term involving only changes in humidity (Fig. 4B) causes increasing  $P-E$  in regions of low level mean mass convergence and decreasing  $P-E$  in regions of low level mean mass divergence, generally intensifying the

existing pattern of  $P-E$  (6). This term helps explain much of the reduction in  $P-E$  over the subtropical oceans where there is strong evaporation, atmospheric moisture divergence and low precipitation (6). Over land areas, in general, there is no infinite surface water source and  $P-E$  has to be positive and sustained by atmospheric moisture convergence. Over the American Southwest, in the current climate, it is the time varying flow that sustains most of the positive  $P-E$  while the mean flow diverges moisture away. Here, the 'humidity contribution' leads to reduced  $P-E$  as the moisture divergence by the mean flow increases with rising humidity. Over the Mediterranean region there is mean moisture divergence and again rising humidity leads to increased mean moisture divergence and reduced  $P-E$ .

Over the ocean the contribution of humidity changes to changes in  $P-E$  can be closely approximated by assuming that the relative humidity remains fixed at its 1950–2000 values (6). Over almost all land areas, and especially over those that have reduced  $P-E$ , the relative humidity decreases in the early 21st century. This is because, unlike over the ocean, evaporation cannot keep pace with the rising saturation humidity of the warming atmosphere. Over land the humidity contribution to the change in  $P-E$  is distinct from that associated with fixed relative humidity.

Decreases in  $P-E$  can also be sustained by changes in atmospheric circulation that alter the mean moisture convergence even in the absence of changes in humidity (Fig. 4A). This 'mean circulation contribution' leads to reduced  $P-E$  at the northern edge of the subtropics (e.g. the Mediterranean region, the Pacific and Atlantic around 30°N and parts of southwestern North America). The change in moisture convergence by the transient eddies (Fig. 4C) dries southern Europe and the subtropical Atlantic and moistens the higher latitude Atlantic but does not have a coherent and large impact over North America.

A significant portion of the mean circulation contribution, especially in winter, can be accounted for by the change in zonal mean flow alone (not shown), indicating that changes in the Hadley Cell and the extratropical mean meridional circulation are important. In summary, increases in humidity and mean moisture divergence, changes in atmospheric circulation and intensification of eddy moisture divergence, cause drying in the subtropics, including over western North America and the Mediterranean region. For the Southwest region, the annual mean  $P-E$  reduces by 0.086 mm/day which is largely accounted for by an increase in the mean flow moisture divergence. Changes in the circulation alone contribute 0.095 mm/day of drying and changes in the humidity alone contribute 0.032 mm/day. This is modestly offset by an increased transient eddy moisture convergence of 0.019 mm/day.(7).

Within models the poleward edge of the Hadley Cell and the mid-latitude westerlies move poleward during the 21st century (8–10). The descending branch of the Hadley Cell causes aridity and hence the subtropical dry zones expand poleward. In models, a poleward circulation shift can be forced by rising tropical SSTs in the Indo-Pacific region (11) and by uniform surface warming (12). The latter results are relevant because the spatial pattern of surface warming in the AR4 models is quite uniform away from the poles. One explanation (13, 14) is that rising tropospheric static stability, an established consequence of moist thermodynamics, stabilizes the subtropical jet streams at the poleward flank of the Hadley Cell to baroclinic instability. Consequently the Hadley Cell extends poleward, increasing the vertical wind shear at its edge, to a new latitude where the shear successfully compensates for the suppression of baroclinic instability by rising static stability.

While increasing stability is likely to be a significant component of the final explanation, a fully satisfying theory for the poleward shift of the zonal mean atmospheric circulation in a warming world must account for the complex interplay between the mean circulation (Hadley Cell and the mid-latitude Ferrell Cell) and the transient eddies (13, 14) that will determine where precipitation will increase and decrease in the future. However not all of the subtropical drying in the Southwest and Mediterranean region can be accounted for by zonally symmetric processes and a full explanation will require attention to moisture transport within localized storm tracks and stationary waves.

The six severe, multiyear, droughts that have struck western North America in the instrumental record have all been attributed, using climate models, to variations of sea surface temperatures (SSTs) in the tropics, particularly persistent La Niña-like SSTs in the tropical Pacific Ocean (15–19). The future climate of intensified aridity in the Southwest is caused by different processes since the models vary in their tropical SST response to anthropogenic forcing. Instead it is caused by rising humidity that causes increased moisture divergence and changes in atmospheric circulation cells that include a poleward expansion of the subtropical dry zones. The drying of subtropical land areas that, according to the models is imminent or already underway, is unlike any climate state we have seen in the instrumental record. It is also distinct from the multidecadal megadroughts that afflicted the American Southwest during Medieval times (20–22) which have also been attributed to changes in tropical SSTs (18, 23). The most severe future droughts will still occur during persistent La Niña events but they will be worse than any since the Medieval period because the La Niña conditions will be perturbing a base state that is drier than any experienced recently (25).

## References and Notes

1. U. Cubasch et al., in *Climate Change 2001 - The Scientific Basis: Contribution of Working Group I to the Third Assessment Report of the Intergovernmental Panel on Climate Change* (Eds. Houghton, J.T. et al.) (Cambridge University Press, 2001), pp. 525–582.
2. M. R. Allen and W. J. Ingram, *Nature* **419**, 224 (2002).
3. Details of the models analyzed can be found at [http://www-pcmdi.llnl.gov/ipcc/model\\_documentation/ipcc\\_model\\_documentation.php](http://www-pcmdi.llnl.gov/ipcc/model_documentation/ipcc_model_documentation.php) and the data at <https://esg.llnl.gov:8443/index.jsp>.
4. N. Nakicenovic, R. Swart (Eds.), *Special Report on Emissions Scenarios* (Cambridge University Press, New York, 2000).
5. T. L. Delworth et al., *J. Climate* **19**, 643 (2006).
6. I. M. Held, B. J. Soden, *J. Climate* **19**, 5686 (2006).
7. The model P–E is not fully accounted for by the computed moisture flow convergence by the sum of the components of the mean flow and transient eddies (the imbalance is 0.022 mm/day). Calculations were performed with daily data on the model grid using closely matching numerics but errors can be introduced by not using sub-daily data and by neglect of moisture diffusion, potentially large over mountains) which was not archived. The data is available at <http://kage.ldeo.columbia.edu/SOURCES/LDEO/ClimateGroup/GFDL>.
8. J. H. Yin, *Geophys. Res. Lett.* doi:10.1029/2005GL023684 (2005).
9. P. J. Kushner, I. M. Held and T. L. Delworth, *J. Climate* **14**, 2238 (2001).
10. L. Bengtsson, K. I. Hodges and E. Roeckner, *J. Climate* **19**, 3518–3543.
11. N.-C. Lau, A. Leetmaa and M. J. Nath, *J. Climate* **19**, 3607 (2006).
12. S. Lee, *J. Atmos. Sci.* **56**, 1353 (1999).
13. T. Schneider, *Ann. Rev. Earth Plan. Sci.* **34**, 655 (2006).
14. C. C. Walker and T. Schneider, *J. Atmos. Sci.* **63**, 3333.
15. S. D. Schubert, M. J. Suarez, P. J. Region, R. D. Koster, J. T. Bacmeister, *Science* **303**, 1855 (2004).
16. S. D. Schubert, M. J. Suarez, P. J. Region, R. D. Koster, J. T. Bacmeister, *J. Climate* **17**, 485 (2004).
17. R. Seager, Y. Kushnir, C. Herweijer, N. Naik, J. Velez, *J. Climate* **18**, 4068 (2005).
18. C. Herweijer, R. Seager and E. R. Cook, *The Holocene* **16**, 159 (2006).
19. H.-P. Huang, R. Seager and Y. Kushnir, *Clim. Dyn.* **24**, 721 (2005).
20. S. Stine, *Nature* **369**, 546 (1994).
21. E. R. Cook, C. A. Woodhouse, M. Eakin, D. M. Meko and D. W. Stahle, *Science* **306**, 1015(2004).
22. C. Herweijer, R. Seager, E. R. Cook and J. Emile-Geay, *J. Climate* **20**, 1353.

23. E. R. Cook, R. Seager, M. A. Cane, D. W. Stahle, *Earth Sci. Rev.* **81**, 93 (2007).

24. This work was supported at LDEO by NOAA grants NA03OAR4320179, NA06OAR4310151, NA03OAR4320179 and NA03OAR4320179, and NSF grants ATM05-01878 and ATM03-47009. We thank R. Dole, W. Robinson, and M. Wallace for useful conversations

5 January 2007; accepted 26 March 2007

Published online 5 April 2007; 10.1126/science.1139601

Include this information when citing this paper.

**Fig. 1:** Modeled changes in annual mean precipitation minus evaporation over the American Southwest ( $125^{\circ}\text{W}$ – $95^{\circ}\text{W}$ ,  $25^{\circ}\text{N}$ – $40^{\circ}\text{N}$ , land areas only) averaged over ensemble members for each of the 19 models. The historical period used known and estimated climate forcings and the projections used the SResA1B emissions scenario. Shown are the median (red line) and 25th and 75th percentiles (pink shading) of the  $P$ – $E$  distribution amongst the 19 models, and the ensemble medians of  $P$  (blue line) and  $E$  (green line) for the period common to all models (1900 to 2098). Anomalies for each model are relative to that model's climatology for 1950–2000. Results have been six year low pass Butterworth filtered to emphasize low frequency variability that is of most consequence for water resources. Units are in mm/day. The model ensemble mean  $P$ – $E$  in this region is around 0.3 mm/day.

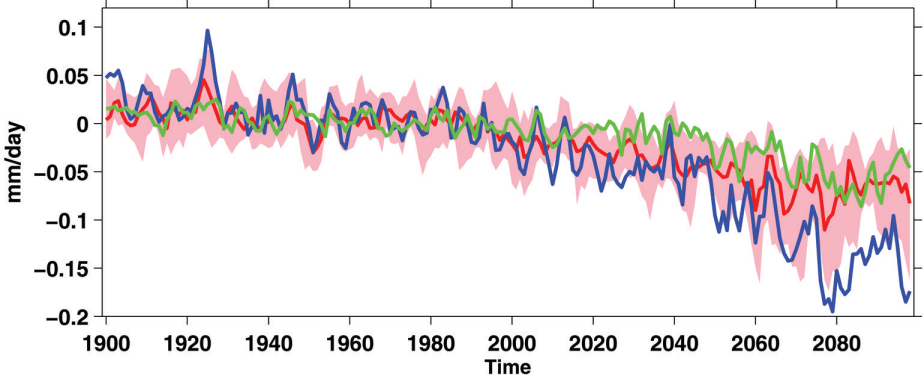
**Fig. 2:** The change in annual mean  $P$ – $E$  over the American Southwest ( $125^{\circ}\text{W}$ – $95^{\circ}\text{W}$ ,  $25^{\circ}\text{N}$ – $40^{\circ}\text{N}$ , land areas only) for 19 models relative to model climatologies for 1950–2000. Results are averaged over twenty year segments of the current century. The number of ensemble members for the projections are listed by the model name at left. Black dots represent ensemble members, where available, and red dots represent the ensemble mean for each model. Units are in mm/day.

**Fig. 3:** The change in annual mean  $P$ – $E$  over the American Southwest ( $125^{\circ}\text{W}$ – $95^{\circ}\text{W}$ ,  $25^{\circ}\text{N}$ – $40^{\circ}\text{N}$ , land areas only) for four coupled models relative to model ensemble mean climatologies for 1950–2000. The results are from individual simulations of the 1860 to 2000 period forced by known and estimated climate forcings and individual projections of future climate using the SResA1B scenarios of climate forcings. Since the modeled anomalies have not been averaged together here these time series provide an idea of plausible evolutions of Southwest climate towards a more arid state. The models are the National Center for Atmospheric Research Community Climate System Model, Geophysical Fluid Dynamics Laboratory model CM2.1, Max Planck Institut Für Meteorologie model ECHAM5 and

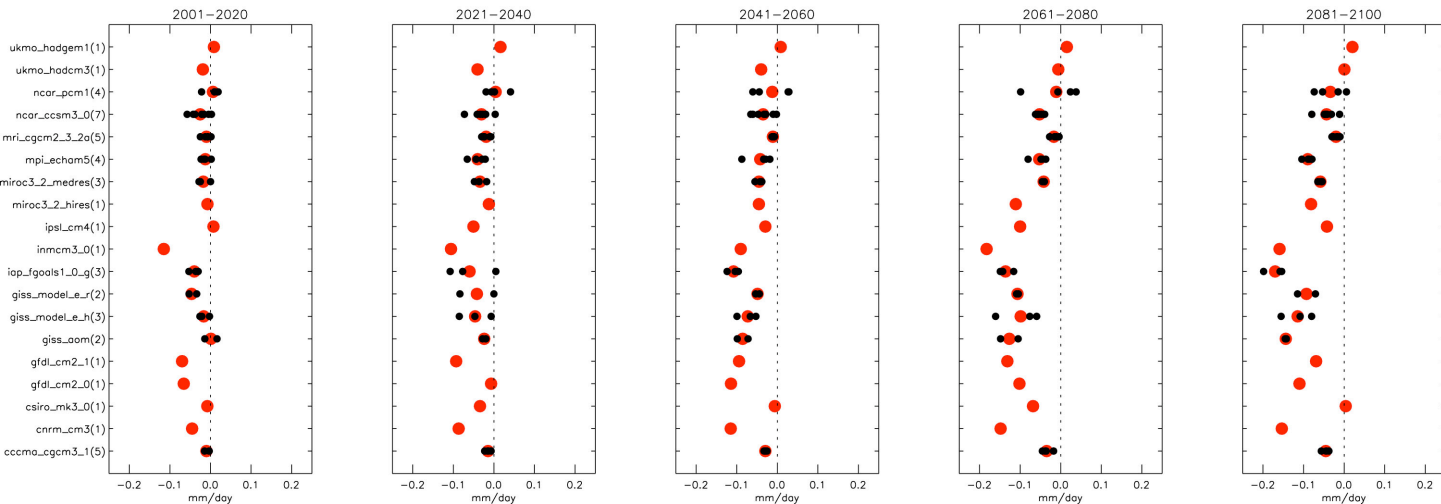
Hadley Centre for Climate Change model HadCM3. All time series are for annual mean data and a six year low pass Butterworth filter has been applied. Units are in mm/day.

**Fig. 4:** The change in annual means of  $P$ – $E$  for 2021–2040 minus 1950–2000 (all panels, contours) and contributions to the change in vertically integrated moisture convergence (colors, negative values imply increased moisture divergence) by the mean flow due to changes in the flow (top), the specific humidity (middle) and the transient eddy moisture convergence (bottom), all for the GFDL CM2.1 model. The box shows the area we define as the “Southwest.”

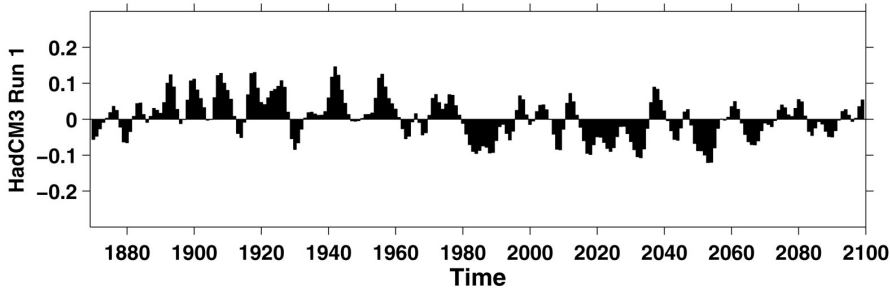
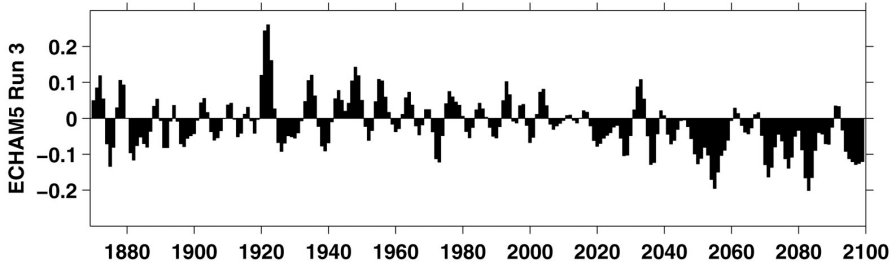
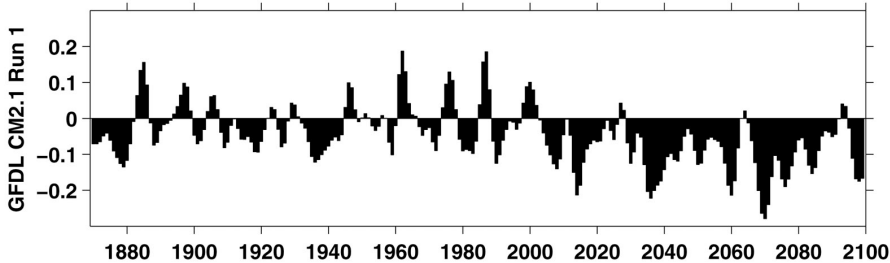
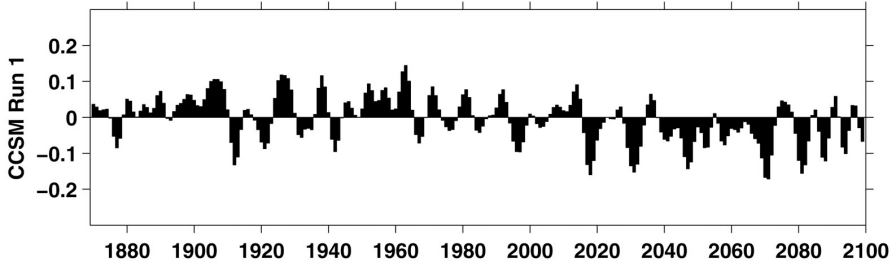
Filtered P-E Anom, Median of 19 models (red), 25th to 75th (pink); 50th P (blue), 50th E (green)



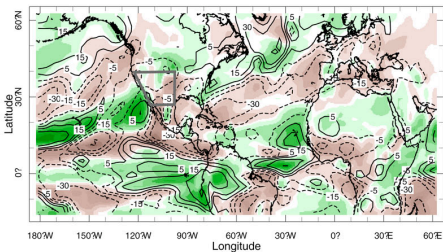
# Precipitation - Evaporation Anomaly(25N-40N,95W-125W)



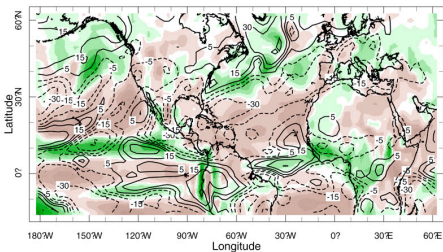
# Filtered Precip–Evap Anomaly (25N–40N, 95W–125W) mm/day



## a) Mean Circulation Contribution



## b) Q Contribution to Mean



## c) Transient Contribution

